Monte Carlo study of the growth of $L1_2$-ordered domains in fcc A_3B binary alloys

Carlos Frontera, Eduard Vives, Teresa Castán, and Antoni Planes
Departament d'Estructura i Constituents de la Matèria, Facultat de Física, Universitat de Barcelona, Avd. Diagonal 647, E-08028 Barcelona, Catalonia, Spain

(Received 1 April 1996; revised manuscript received 26 June 1996)

A Monte Carlo study of the late time growth of $L1_2$-ordered domains in a fcc A_3B binary alloy is presented. The energy of the alloy has been modeled by a nearest-neighbor interaction Ising Hamiltonian. The system exhibits a fourfold degenerated ground state and two kinds of interfaces separating ordered domains: flat and curved antiphase boundaries. Two different dynamics are used in the simulations: the standard atom-atom exchange mechanism and the more realistic vacancy-atom exchange mechanism. The results obtained by both methods are compared. In particular we study the time evolution of the excess energy, the structure factor and the mean distance between walls. In the case of atom-atom exchange mechanism anisotropic growth has been found: two characteristic lengths are needed in order to describe the evolution. Contrarily, with the vacancy-atom exchange mechanism scaling with a single length holds. Results are contrasted with existing experiments in Cu_3Au and theories for anisotropic growth. [S0163-1829(97)08801-2]

I. INTRODUCTION

Kinetics of phase transitions is a problem of great interest not only because its fundamental importance in nonequilibrium statistical physics, but also because its many implications in different areas of material science and technology.[1,2] The phenomenon is a consequence of the far from-equilibrium initial conditions induced by the sudden change of the imposed thermodynamic parameters on time scales much shorter than the time scales characterizing the process towards the equilibrium situation. Typically, the system is quenched through its equilibrium ordering temperature. Immediately after the quench, domains of the ordered phase appear. As time goes on, they grow in size in order to reduce the excess free energy of the walls. This growth shows distinct regimes from early to late times. At late times, in the so-called domain-growth regime, it is usually assumed that the domain size is much larger than all microscopic lengths in the system. Then, inspired by the situation in equilibrium critical phenomena, it is assumed that the system shows dynamical scaling.[3] This means that at different times the domain structure looks the same when lengths are measured in units of the characteristic length. Furthermore, the average domain size is supposed to increase with time according to a power law with an exponent n characteristic of the universality class to which the system is supposed to belong.[4] If these universality classes really exist, the important point is to identify the distinctive features of a given class. In the simplest case, they are supposed to depend only on whether or not the order parameter is conserved. A typical example for the conserved case is a phase separation process while an order-disorder transition in a binary alloy corresponds to the nonconserved situation. In the first case $n=1/3$ has been predicted while $n=1/2$ is the expected value in the second case.[1] Nevertheless, the concept of universality is not firmly established and is still under discussion. The above classification, just based on the order parameter conservation property, seems to apply only when no disorder is present in the system and the excitations are homogeneously distributed. For instance it is well acknowledged that quenched disorder gives rise to logarithmic growth-laws,[5] and that excitations localized on the interfaces give rise to exponents greater than 1/2 and 1/3 for the nonconserved and conserved cases, respectively.[6,7] Moreover other parameters such as the ground-state degeneracy, nonstoichiometry or anisotropic effects could modify the exponents. The exponent $n=1/2$ in nonconserved order parameter systems is theoretically based on a curvature-driven interface motion.[8] This is the well-known Allen-Cahn growth law. A special curvature driven case leading to an exponent $n=1/4$ has been found for anisotropic systems with a mixture of perfectly flat and curved domain walls.[9]

In this paper we will focus on the domain-growth problem in a fcc A_3B binary alloy undergoing an order-disorder transition from a disordered to a $L1_2$ structure. This has been the system most widely used to perform experiments intended to study ordering kinetics in nonconserved order parameter systems.[10–18] In spite of that, theoretical studies of domain growth in fcc systems are really scarce and, as far as we know, only a recent paper by Lai[19] is specifically devoted to the study of such kind of systems. Concerning computer simulation no data has, to our knowledge, been published. This is a rather surprising fact since Monte Carlo simulations have been of seminal importance in providing much of the quantitative insight into ordering kinetic problems. This is probably due to the complexity of ordering problems in fcc lattices and also to the demanding computer time. Actually the ground state is fourfold degenerate and there exist two different kinds of antiphase boundaries: high and low excess-energy boundaries. Then, two characteristic lengths may grow following different laws (anisotropic growth) and this can, in some way, question the validity of scaling properties in such a system. In fact, related problems have been considered in two-dimensional lattices. For example, the fcc problem has some similarities with the problem of island growth in a system of hydrogen adsorbed on a (110) iron surface with coverage 2/3.[20] In this case an exponent smaller than 1/2, which is indicative of interface diffusion effects, has

 © 1997 The American Physical Society

been found. Also some indications on anisotropic growth are reported in the same reference.[20] Concerning the experimental situation, among a rich literature, it is worth mentioning the pioneer x-ray diffraction work by Cowley[21] devoted to the study of the superstructure peak in Cu_3Au single crystals close to equilibrium. Much more recently, a very complete time-resolved x-ray scattering study in a single crystal of Cu_3Au,[18] has been published. The authors obtain $n=1/2$ with a high degree of accuracy for the growth of the high energetic boundaries and with less accuracy for the low energetic ones. This led them to the conclusion that scaling holds in this anisotropic system in agreement with the theoretical predictions by Lai.[19]

Our interest in this paper is to present extensive Monte Carlo simulations of the domain-growth process performed in a fcc A_3B alloy. Since we model the system assuming pairwise interactions between nearest-neighbor atoms only, the low-energy boundaries have exactly zero excess energy. We expect that this extreme situation emphasizes any tendency of the system to show anisotropic growth effects. In addition we will perform simulations in systems either with and without vacancies (in this last case only vacancy-atom exchanges will be allowed) in order to investigate the effect of the vacancy mechanism in the kinetics of ordering in fcc lattices. This mechanism has been shown to play a very important role in bcc lattices.[22,23]

We have restricted the present study to stoichiometric alloys. It is known that the coupling between the order parameter and the excess of concentration gives rise to interesting phenomena.[24,25] Moreover, in fcc binary alloys, nonstoichiometry may also favor the apparition of modulated phases.[26]

The paper is organized as follows. In the next section we introduce the model and describe some of the features of the ground state and the domain walls. In Sec. III we explain the details of the Monte Carlo simulations and define the different magnitudes used to describe the ordering process. The results are presented in Sec. IV and discussed in Sec. V. Finally, in Sec. VI, we give a summary of the main conclusions.

II. MODEL AND GROUND STATE

The binary alloy is modeled by a set of N_A A atoms, N_B B atoms, and N_V vacancies on a ''perfect'' fcc lattice with spacing a, linear size aL, and periodic boundary conditions. The number of lattice sites is $N=4L^3=N_A+N_B+N_V$. Assuming nearest-neighbors (NN) interactions only, a general ABV Hamiltonian[27] can be written as a Blume-Emery-Griffiths[28] model, as explained in Refs. 23,29. In the case of low vacancy concentrations ($N_V \ll N_A, N_B$) this Hamiltonian can be approximated by a spin-1 Ising model:

$$\mathcal{H}=J\sum_{\langle i,j\rangle}^{\mathrm{NN}} S_i S_j, \tag{2.1}$$

where the sums extend over all NN pairs and i and j are generic indexes sweeping all the lattice ($i,j=1,\ldots N$). The spin variables S_i can take three values: $+1$, -1, and 0 when the ith position of the lattice is occupied by an A atom, a B atom, or a vacancy, respectively.

We have focused on the case $N_A \simeq 3N_B \gg N_V$ in order to simulate an A_3B alloy such as Cu_3Au, with little concentration of vacancies. It is well known that for $J>0$ and no vacancies ($N_V=0$) this system exhibits a discontinuous order-disorder phase transition when temperature is increased.[30–32] The ordered phase is the so-called $L1_2$ structure. Hamiltonian (2.1) without vacancies has been repeatedly used to model such order-disorder transition in metallic alloys (see Ref. 32 and references therein). Regarding the fcc lattice as four interpenetrated simple cubic sublattices (named α, β, γ, and δ); the perfect $L1_2$ order consists in three sublattices occupied by A species whereas the other one is occupied by B species so that it is fourfold degenerated. The four equivalent kinds of ordered domains will be called α, β, γ, and δ domains according to the sublattice which contains the minority species B. The order is described by means of the three following long-range order parameters:[19]

$$\Psi_1=\frac{2}{N}\sum_{ijk\xi\eta\zeta} S_{ijk\xi\eta\zeta}(-1)^{\xi},$$

$$\Psi_2=\frac{2}{N}\sum_{ijk\xi\eta\zeta} S_{ijk\xi\eta\zeta}(-1)^{\eta},$$

$$\Psi_3=\frac{2}{N}\sum_{ijk\xi\eta\zeta} S_{ijk\xi\eta\zeta}(-1)^{\zeta}, \tag{2.2}$$

where $S_{ijk\xi\eta\zeta}$ is the spinlike variable at position $\vec{r}_{ijk\xi\eta\zeta}=a(i+\xi/2,j+\eta/2,k+\zeta/2)$; i,j,k range from 1 to L and the vector (ξ,η,ζ) takes the values (0,0,0), (0,1,1), (1,0,1), and (1,1,0) pointing to the position of the four sublattices α, β, γ, and δ, respectively.

After a quench through the equilibrium transition temperature T_0, the four possible degenerated domains appear and compete during the domain-growth regime. It is well known[11,33,34] that two kinds of antiphase domain boundaries (APDB) exist:

(1) The first type (named type-1 or ''half diagonal glide'' walls) of APDB corresponds to a displacement vector contained in the plane of the APDB. This kind of boundaries maintains the same number of $A-B$ NN bonds as in the ordered bulk. Hence, in our model with NN interactions only, such boundaries do not suppose any excess of energy. It is also interesting to remark that they can only appear in specific directions depending on the two adjacent domains: for instance they can appear perpendicular to direction [100] between α and β domains and between γ and δ domains. Table I shows the directions of the type-1 walls for all the possible neighboring domains. Moreover, it is possible to build up a structure combining the different kinds of ordered domains with only type-1 walls, i.e., without excess of energy. At low temperatures, such structure would not evolve in time.

(2) The second type of APDB (type-2 walls) corresponds to a displacement vector not contained in the boundary plane. Since it does not conserve the number of $A-B$ NN bonds as in the bulk, it contributes with a positive excess of energy. It should also be mentioned that these boundaries contain a local excess of particles (either A or B).

TABLE I. Directions of the nonenergetic type-1 walls between possible pairs of neighboring domains.

(Ψ_1,Ψ_2,Ψ_3)	α $(-1,-1,-1)$	β $(-1,1,1)$	γ $(1,-1,1)$	δ $(1,1,-1)$
α		[100]	[010]	[001]
β	[100]		[001]	[010]
γ	[010]	[001]		[100]
δ	[001]	[010]	[100]	

III. MONTE CARLO SIMULATION DETAILS

A. Dynamics

We have performed two kinds of simulation studies:

(1) The first kind includes the simulations of the ordering processes without vacancies ($N_V=0$), which have been performed using the standard Kawasaki dynamics proposing exchanges between NN atoms.

(2) The second kind includes the simulations with vacancies. In this case we have used a restricted Kawasaki dynamics proposing NN vacancy-atom exchanges (vacancy jumps) only. This dynamics is more realistic, in the sense that, although approximately, it takes into account the role played by vacancies in ordering kinetics in binary alloys. The concentration of vacancies has been taken the same in all the simulations ($c_V \equiv N_V/N \simeq 3.1\times 10^{-5}$).

By both dynamics, the concentration of particles is preserved while the order parameters are not. In both cases we have accepted or refused the proposed exchange using the usual Metropolis acceptance probability:

$$p(\Delta\mathcal{H})=\begin{cases} 1 & \text{if } \Delta\mathcal{H}\leqslant 0, \\ \exp\left\{-\dfrac{\Delta\mathcal{H}}{k_BT}\right\} & \text{if } \Delta\mathcal{H}>0, \end{cases} \tag{3.1}$$

where $\Delta\mathcal{H}$ is the energy change associated with the proposed exchange. We define the unit of time, the Monte Carlo step (mcs), as the trial of N exchanges (either atom-atom or vacancy-atom exchanges). In all the cases we have started the simulations from a completely disordered state, which would correspond to the configuration of a system at $T=\infty$. The system is then rapidly quenched at a final temperature T_q below the transition temperature T_0. To prepare the disordered states we fill up the system with A atoms and randomly replace $N/4$ of them by B atoms; when it is necessary, we also choose at random N_V lattice sites to place the vacancies.

B. Measures of growth

Our main interest is the description of the time evolution of the ordered domains. Usually, the domain size is measured as the inverse of the excess energy, which is proportional to the total amount of interface.[35] Nevertheless, in our case, there are two coexisting types of interfaces and only the total amount of type-2 walls might be related to the excess energy since type 1 does not contribute to the excess-energy. Consequently for fcc lattices with $L1_2$ order it is convenient to simultaneously measure both the excess energy and the structure factor. These two quantities are defined as follows:

(1) Excess energy per site:

$$\Delta E(t)\equiv\frac{1}{N}[\mathcal{H}(t)-\mathcal{H}(t\rightarrow\infty)], \tag{3.2}$$

where $\mathcal{H}(t\rightarrow\infty)$ is the equilibrium energy at the quenching temperature T_q.

(2) Structure factor:

$$S(\vec{k},t)\equiv\left|\frac{1}{N}\sum_{ijk\xi\eta\zeta}S_{ijk\xi\eta\zeta}\exp\left(\mathbf{i}\frac{2\pi}{a}\vec{k}\cdot\vec{r}_{ijk\xi\eta\zeta}\right)\right|^2, \tag{3.3}$$

where the sum extends over the whole lattice, **i** is the imaginary constant, and $\vec{k}$ is the dimensionless reciprocal vector. The discreteness of the real space makes the structure factor to be invariant under the $\langle 200\rangle$ translations in the reciprocal space. The periodic boundary conditions imply that the reciprocal space is discrete on a cubic lattice on the $\vec{k}$ space with spacing $1/L$. Figure 1 shows the reciprocal space with the position of the fundamental and the superstructure peaks.

C. Domains and superstructure peak

The temporal evolution of the domain structure is illustrated in Figs. 2(a)–2(c). Three snapshots, at selected times, corresponding to a section parallel to the (100) planes are presented. The four different ordered regions are indicated with different colors. Flat (type-1) and curved (type-2) interfaces can be observed. It is worth mentioning the similarities between such snapshots and the experimental results obtained for Cu_3Au using dark field microscopy technique.[36] The mean distance between such walls is related to the shape of the superstructure peaks of the structure factor. Discrepancies in the shape of these peaks have been reported in the literature. Old x-ray measurements by Cowley[21] suggested that the peaks are square shaped. More recently it has been suggested that the peaks are disk shaped.[18] Our simulations give square (or even starlike) shaped peaks as it can be seen

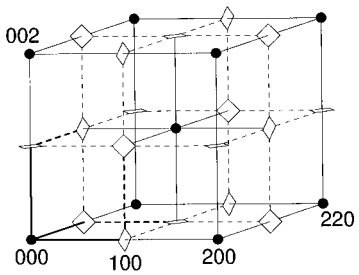

FIG. 1. Reciprocal $\vec{k}$ space showing the fundamental (filled circles) and the superstructure (squares) peaks. The average of the structure factor on the thick solid lines is $S_r(q,t)$ and the average on the thick dashed lines is $S_t(q,t)$.

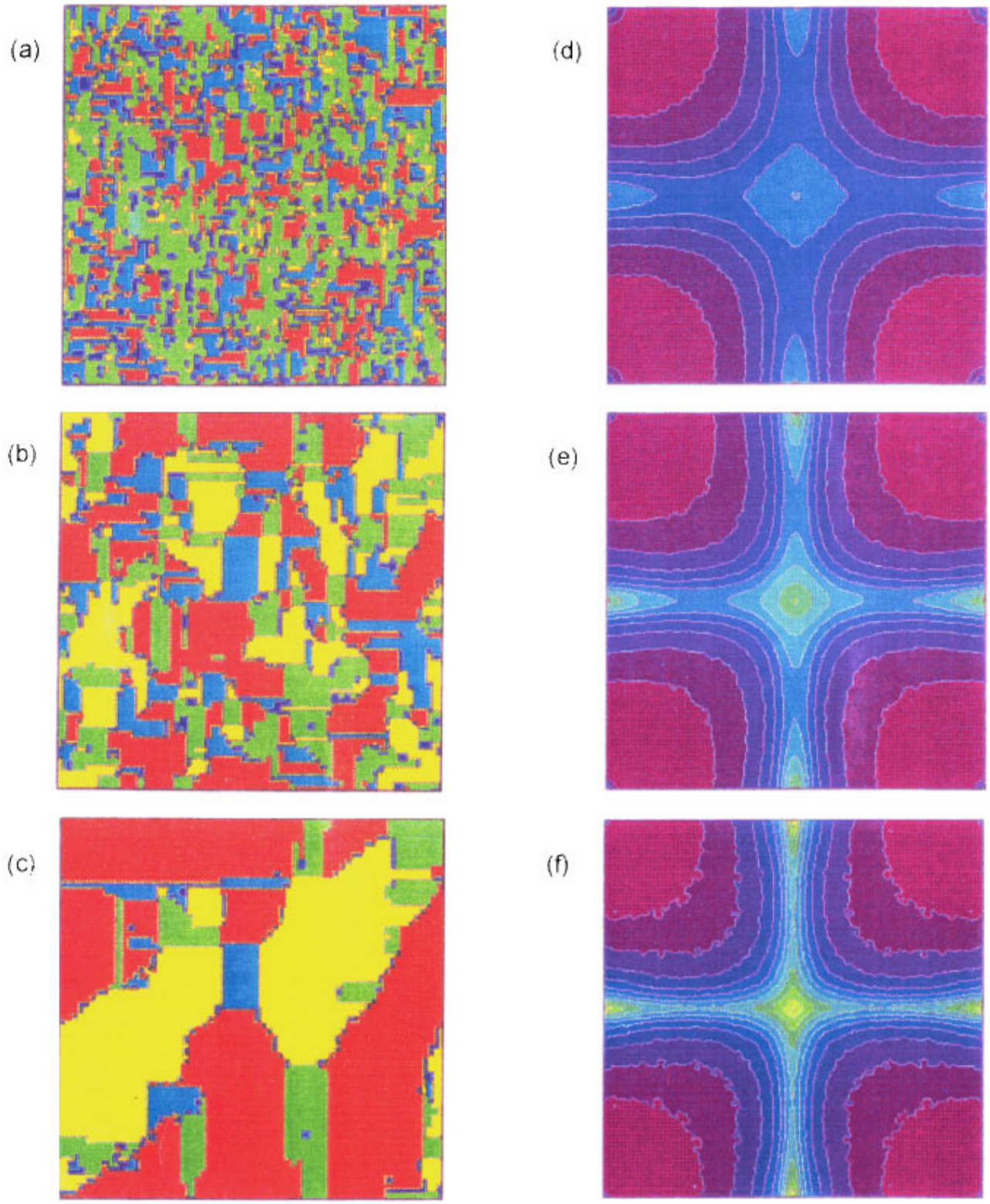

FIG. 2. Snapshots of the system evolution in real space [(a), (b), and (c)] and in reciprocal space [(d), (e), and (f)]. The real space pictures, corresponding to a section perpendicular to (100) direction, show in four different colors the structure of ordered domains. The reciprocal space maps show the logarithm of the structure factor in the (100) plane. Color scale increases from violet to yellow. Data corresponds to a simulation using the atom-atom exchange mechanism at $T_q = 1.0$, system size $L = 64$, and times $t = 18$ mcs [(a) and (d)], $t = 198$ mcs [(b) and (e)] and $t = 1998$ mcs [(c) and (f)].

in the temporal sequence presented in Figs. 2(d)–2(f). Such anisotropy in the peak shape does not necessarily imply that the ordered domains are needle shaped, but arises from the correlation between the ordered domains. For instance the superstructure peak at the (100) position accounts for the long-range order parameter Ψ_1. This order parameter does not discriminate between α and β domains (both having $\Psi_1 = -1$) nor between γ and δ domains (both having

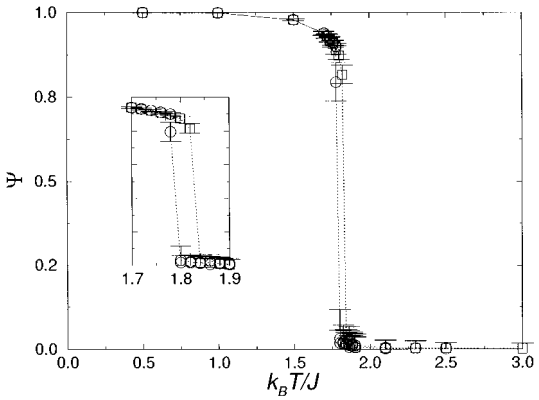

FIG. 3. Equilibrium order parameter as a function of temperature for $L=20$ using atom-atom exchange mechanism. The inset shows in detail the hysteresis due to the discontinuous character of the transition. It can be concluded that $k_BT_c/J=1.81\pm0.03$. Squares correspond to a heating process while circles to a cooling one.

$\Psi_1=1$). The tendency of the domains to locate in such a way that the interface does not have extra energy favors the formation of α-β and γ-δ boundaries (type 1) perpendicular to the [100] direction. Therefore the regions with a high value of the order parameter Ψ_1 are anisotropic, producing the anisotropy of the (100) peak. The same happens for the other peaks at (010) and (001).

The inverse of the amplitudes of the superstructure peak along both, the radial (σ_r) and the transverse (σ_t) directions, are related to the mean distance between type-2 and type-1 walls, respectively. The measurement of σ_r has been done by analyzing the profile of

$$S_r(q,t)=\frac{1}{3}\left[S\left((1,0,0)-\frac{1}{L}(q,0,0),t\right)+S\left((0,1,0)-\frac{1}{L}(0,q,0),t\right)+S\left((0,0,1)-\frac{1}{L}(0,0,q),t\right)\right], \tag{3.4}$$

where $q=0,1,\ldots,L$ is the distance from the superstructure peak (in units of $1/L$). Following the notation in Ref. 18, we will refer to this profile as the radial scan of the structure factor. It corresponds to the average on the three thick continuous lines of Fig. 1. The measurement of σ_t has been done by analyzing the profile of

$$S_t(q,t)=\frac{1}{6}\left[S\left((1,0,0)+\frac{1}{L}(0,0,q),t\right)+S\left((1,0,1)-\frac{1}{L}(0,0,q),t\right)+S\left((0,1,0)+\frac{1}{L}(q,0,0),t\right)+S\left((1,1,0)-\frac{1}{L}(q,0,0),t\right)+S\left((0,0,1)+\frac{1}{L}(0,q,0),t\right)+S\left((0,1,1)-\frac{1}{L}(0,q,0),t\right)\right], \tag{3.5}$$

where $q=0,1,\ldots,L/2$. We will refer to it as a transverse scan of the structure factor. It corresponds to the average on the two symmetric parts of the three thick dashed lines of Fig. 1. It can be easily shown that due to the symmetries of the structure factor the average over the continuous (dashed) thick lines is equal to the average over all the continuous (dashed) lines of Fig. 1. In addition, at every time both profiles have been averaged over a certain number of independent runs (about 25 for $L=64$ and 40 for the other system sizes). This last average is indicated by means of angular brackets ($\langle\cdots\rangle$). The finite-size effects have been studied by simulating systems of linear sizes $L=20$, 28, 36, and 64 ($N=32\,000$, 87 808, 186 624, and 1 048 576 sites, respectively). We have also preliminarily studied the effect of the quenching temperature by performing simulations at $T_q=1.0J/k_B$ ($T_q/T_0\simeq0.55$) and $T_q=1.5J/k_B$ ($T_q/T_0\simeq0.83$).

D. Fitting procedure for σ_r and σ_t

We have measured σ_r and σ_t using the two following methods.

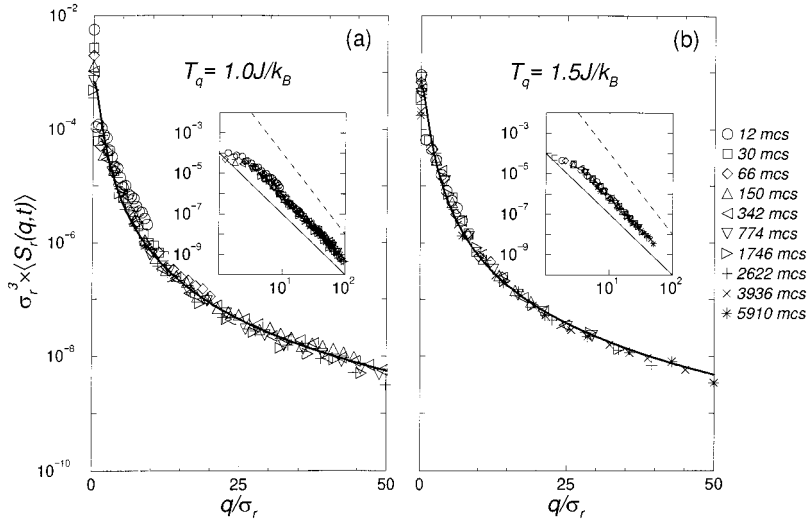

FIG. 4. Linear-log and log-log (insets) plots of the scaled radial scan of the structure factor at different times and quenching temperatures $T_q=1.0J/k_B$ (a) and $T_q=1.5J/k_B$ (b). Data corresponds to systems of linear size $L=64$ for the atom-atom exchange mechanism. The solid thick line corresponds to a fit of expression (3.7) with $\alpha=1.5$ and $\sigma=1$. The dashed lines in the insets show the Porod's law $\tilde{S}_r(\tilde{q})\sim\tilde{q}^{-4}$, while solid lines show the slope of $\tilde{q}^{-3}$.

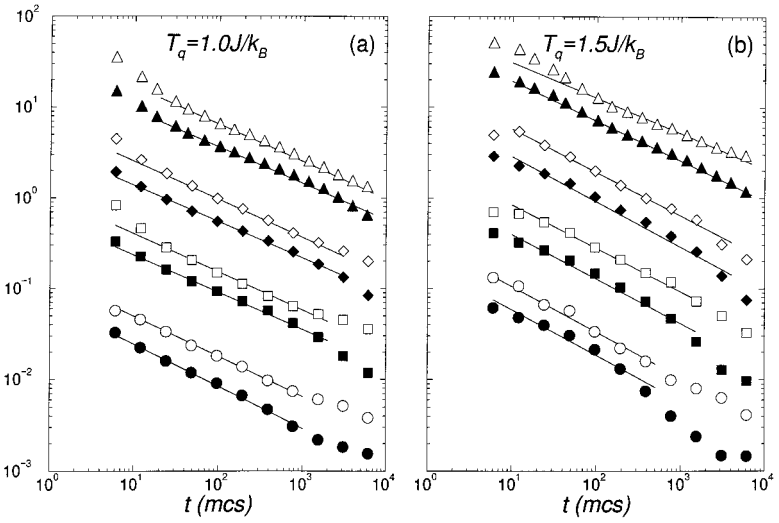

FIG. 5. Time evolution, in the case of atom-atom exchange mechanism, of $\langle \Delta E(t) \rangle$ (filled symbols) and of $\sigma_r(t)$ (open symbols), for $T_q = 1.0J/k_B$ (a) and $T_q = 1.5J/k_B$ (b) for systems of $L = 20$ (circles), $L = 28$ (squares), $L = 36$ (diamonds), and $L = 64$ (triangles). The solid lines are the best power-law fits. Data corresponding to different sizes have been vertically shifted to clarify the picture.

(1) The first method is based on the evaluation of the second moment of the scan:

$$\sigma^2(t) \equiv \frac{\Sigma_{q=0}^{q_{\max}} q^2 \langle S(q,t) \rangle}{\Sigma_{q=0}^{q_{\max}} \langle S(q,t) \rangle}, \tag{3.6}$$

where S represents either S_r or S_t, and $q_{\max}$ is the first q value for which $\langle S(q,t) \rangle$ is lower than a background threshold. The value of this background has been taken as twice the mean value of the structure factor of a completely disordered system (excluding the fundamental peak).

(2) The second method is based on the fitting of a Lorentzian function to the data of the corresponding scan. In order to account for the large-q tail of the structure factor we have fitted $\log\langle S(q,t) \rangle$ to the three-parameters (a,σ,B) function:

$$\log\langle S(q,t) \rangle \simeq \log\left\{ \frac{a}{\left[1 + \left(\frac{q}{\sigma(t)}\right)^2\right]^{\alpha}} + B \right\}, \tag{3.7}$$

where σ is an estimation of the width, B is the background, a is the fitted intensity and α is an exponent (not fitted) that we discuss in the next paragraph.

We have analyzed the validity of both methods for the two scans of the structure factor. The first method turns out to be adequate only for the radial scans. This is because the large-q tail of the transverse scan decays very slowly and, therefore, σ_t is strongly affected by the choice of $q_{\max}$. The second method can be used for both scans. Moreover, both methods give equivalent results for radial scans. Therefore we will estimate σ_r using method 1 and σ_t using method 2. Concerning the exponent α we have tried $\alpha = 1$, 2, and 3/2 for both scans. In general the best fits to the radial scan have been obtained with $\alpha = 3/2$, while for the transverse scans $\alpha = 1$ gives the best results.

E. Dynamical scaling

We have tested the existence of dynamical scaling in both the radial and the transverse directions by plotting the corresponding scaling function $\tilde{S}(\tilde{q})$ defined from the following expression:

$$\langle S(q,t) \rangle = \frac{1}{\sigma(t)^d} \tilde{S}(\tilde{q}), \tag{3.8}$$

where $\tilde{q} = q/\sigma(t)$ is the scaling variable and $d(=3)$ is the dimensionality of the space. Scaling has been tested by

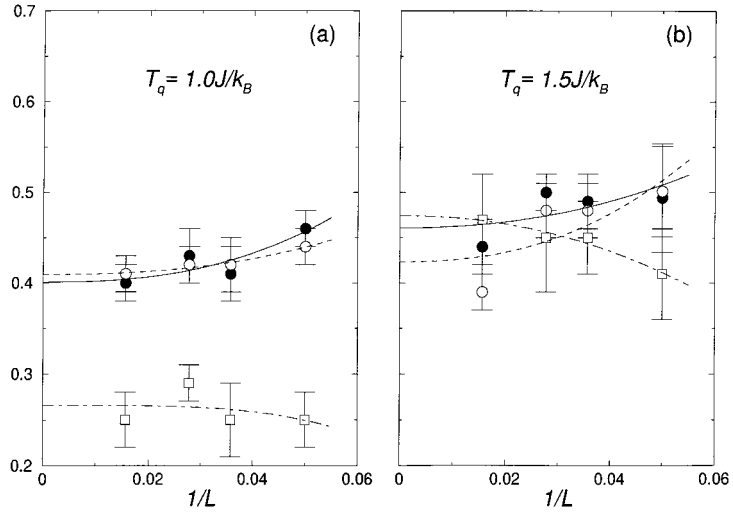

FIG. 6. Exponents x (●) from the excess energy per site (ΔE), y (○) from the second moment of the radial scan of the superstructure peak σ_r and z (□) from the fitted amplitude of the transverse scan of the superstructure peak σ_t, as functions of $1/L$ with the atom-atom exchange mechanism. Data correspond to temperature $T_q = 1.0J/k_B$ (a) and $T_q = 1.5J/k_B$ (b). Lines show the best fits of Eq. (5.2) to the exponents x (solid), y (dashed), and z (dot-dashed).

TABLE II. Fitted exponents of the power-law evolution of the excess energy per site (ΔE), of the second moment of the radial scan (σ_r) and of the fitted amplitude of the transverse scan (σ_t). Data correspond to simulations with the atom-atom exchange mechanism.

k_BT_q/J	L	20	28	36	64	$L\to\infty$
1.0	ΔE	0.46±0.02	0.41±0.03	0.43±0.03	0.40±0.02	0.40±0.03
	σ_r	0.44±0.02	0.42±0.03	0.42±0.02	0.41±0.02	0.41±0.03
	σ_t	0.25±0.03	0.25±0.04	0.29±0.02	0.25±0.03	0.26±0.04
1.5	ΔE	0.50±0.06	0.49±0.03	0.50±0.02	0.44±0.03	0.46±0.06
	σ_r	0.50±0.05	0.48±0.03	0.48±0.03	0.39±0.02	0.42±0.05
	σ_t	0.41±0.05	0.45±0.04	0.45±0.06	0.47±0.05	0.47±0.06

checking the overlap of the data corresponding to different times and also to different system sizes. Theoretical predictions for the scaling function $\tilde{S}(\tilde{q})$ are available,[3,19] especially concerning the behavior for large values of q.

IV. RESULTS

For the sake of clarity the results are presented in the following order: first, the results corresponding to equilibrium simulations (Sec. IV A); second, those concerning the evolution of the system using the atom-atom exchange mechanism (Sec. IV B); and third, the results obtained by means of the vacancy-atom exchange mechanism (Sec. IV C). The results in Secs. IV B and IV C are always given at quenching temperatures $T_q=1.0J/k_B$ and $T_q=1.5J/k_B$. The structure factor profiles are only presented for $L=64$ although data corresponding to smaller L have also been analyzed.

A. Equilibrium

Starting from perfectly ordered systems with $L=20$, we have step-by-step heated them from $T=0.5J/k_B$ to $T=3.0J/k_B$ and cooled them again down to $T=0.5J/k_B$. At each temperature we have let the system reach equilibrium (after $\sim 12\times 10^3$ mcs) and have obtained the equilibrium energy $\mathcal{H}(t\to\infty)$ and the mean long-range order parameter defined as

$$\Psi \equiv \frac{|\Psi_1|+|\Psi_2|+|\Psi_3|}{3}. \tag{4.1}$$

The temporal average of this order parameter is presented in Fig. 3 as a function of temperature. No differences have been found between the presented case corresponding to $N_V=0$ (with the atom-atom exchange mechanism) and the case with $N_V=1$ (with the vacancy-atom exchange mechanism). Our results confirm that the transition is first order and that the heating-cooling cycle shows hysteresis. The transition temperature has been estimated to be $T_0=1.81\pm 0.03J/k_B$ compatible with the Monte Carlo results given in Ref. 32.

B. Atom-atom exchange mechanism

Figures 4(a) and 4(b) show the profiles, at different times, of the radial scan of the structure factor for the two studied quenching temperatures, scaled according to Eq. (3.8). In general, the overlap of the different curves is quite good. It has been checked that data corresponding to different system

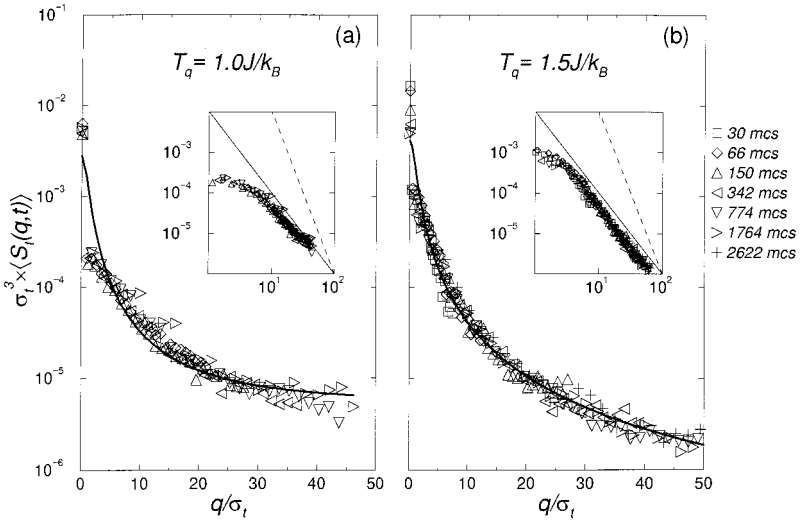

FIG. 7. Linear-log and log-log (insets) plots of the scaled transverse scan of the structure factor at different times and quenching temperatures $T_q=1.0J/k_B$ (a) and $T_q=1.5J/k_B$ (b) with atom-atom exchange mechanism. Data correspond to systems of linear size $L=64$. The solid thick lines correspond to fits of expression (3.7) with $\alpha=1$ and $\sigma=1$. The dashed lines in the insets show the Porod's law $\tilde{S}(\tilde{q})\sim\tilde{q}^{-4}$, while the solid lines show the slope of $\tilde{q}^{-2}$.

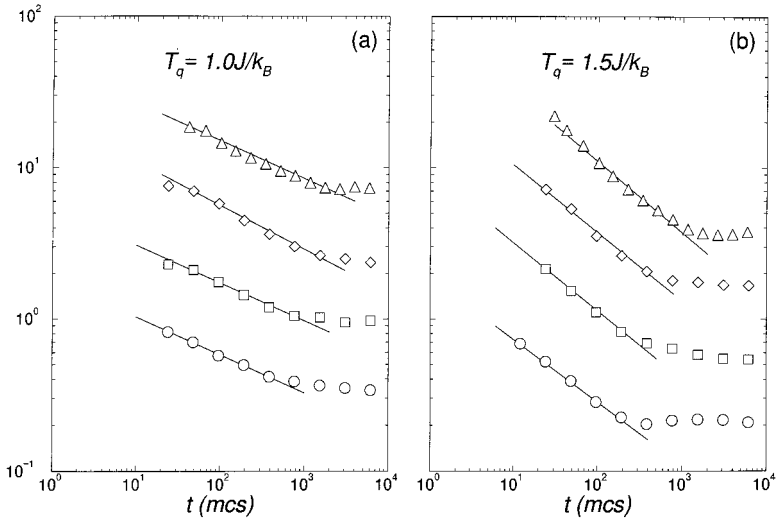

FIG. 8. Log-log plot of the mean distance between type-1 walls for $L=20$ (○), $L=28$ (□), $L=36$ (◇), $L=64$ (△) with atom-atom exchange mechanism. Data correspond to quenching temperatures $T_q=1.0J/k_B$ (a) and $T_q=1.5J/k_B$ (b). Solid lines show the best power-law fits.

sizes also fall on the same curve. Nevertheless, deviations from this scaling can be well appreciated at $q=0$ in Fig. 4(a) ($T_q=1.0J/k_B$). We will come back to this point in the discussion. The continuous lines show fits of Lorentzian functions [Eq. (3.7)] with $\alpha=3/2$ and $\sigma=1$ which corroborates the validity of such kind of fitting function for all the individual profiles. The insets in Figs. 4(a) and 4(b) display log-log plots of the scaled radial scans: for large $\tilde{q}$ values $\tilde{S}_r(\tilde{q})$ decays as $\tilde{q}^{-3}$, as indicated by a continuous line.

Figures 5(a) and 5(b) show log-log plots of the time evolution of $\langle \Delta E(t) \rangle$ and $\sigma_r(t)$ for different system sizes and the two studied quenching temperatures. Solid straight lines are the following fitted power laws:

$$\langle \Delta E(t) \rangle \sim t^{-x},$$

$$\sigma_r(t) \sim t^{-y}. \tag{4.2}$$

The behavior of the growth-exponents x and y for the two quenching temperatures are presented in Fig. 6 as a function of $1/L$. The corresponding numerical values are listed in Table II. The estimations of the two growth exponents, x and y, are coincident within the error bars. A general tendency of the exponent to increase when temperature is increased and to decrease when increasing the system size is observed. Extrapolation to $L\to\infty$, following the method explained in Sec. V, renders $x\simeq y\simeq 0.40$ for $T_q=1.0J/k_B$ and $x\simeq y\simeq 0.44$ for $T_q=1.5J/k_B$.

Figure 7 shows linear-log plots of the transverse scan of the scaled structure factor for the two studied quenching temperatures, at different times. The overlap of the curves is rather satisfactory, however it is not as broaden in time as for the radial scan case. Note that in Fig. 7(b) the lack of scaling at $q=0$ is clearly evident. As for the radial scan case, we have also verified the overlap of the data corresponding to systems with different sizes. The continuous lines show fits of Lorentzian functions [Eq. (3.7)] with $\alpha=1$ and $\sigma=1$. The insets display log-log plots of these scaled transverse scans: in this case $\tilde{S}_t(\tilde{q})$ decays as $\tilde{q}^{-2}$ for large $\tilde{q}$, as indicated by the continuous line.

Log-log plots of the time evolution of $\sigma_t(t)$ for different system sizes and the two studied quenching temperatures are presented in Fig. 8. Solid straight lines correspond to the fitted power law:

$$\sigma_t(t) \sim t^{-z}. \tag{4.3}$$

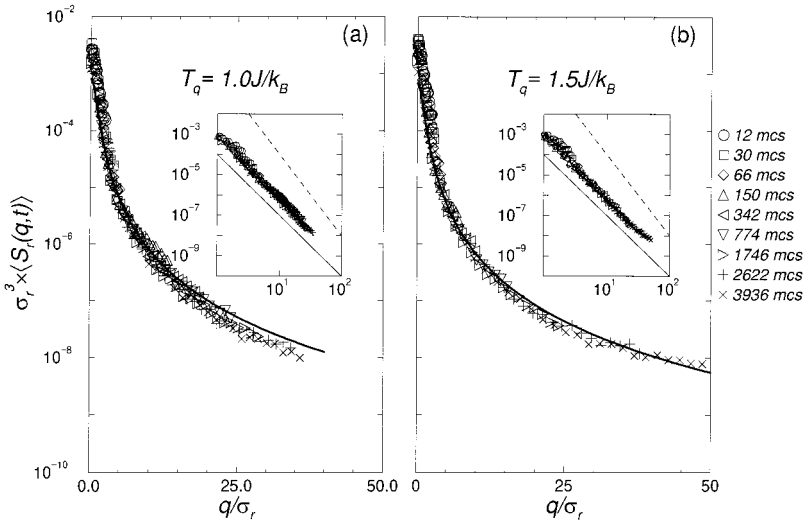

FIG. 9. Same as for Fig. 4 but for the vacancy-atom exchange mechanism.

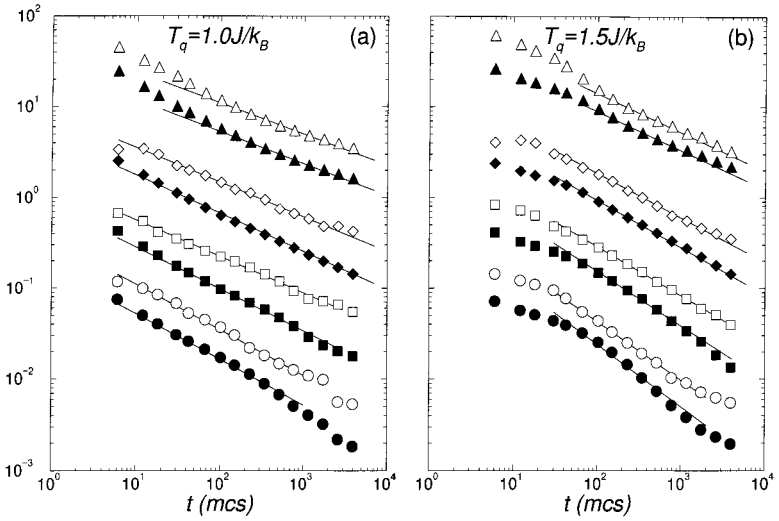

FIG. 10. Same as for Fig. 5 but for the vacancy-atom exchange mechanism.

The values of the growth exponents are listed in Table II and plotted in front of $1/L$ in Fig. 6. In this case, the extrapolations to $L\to\infty$ (following the method explained in Sec. V) render $z\simeq 0.26$ for $T_q=1.0J/k_B$ and $z\simeq 0.47$ for $T_q=1.5J/k_B$.

C. Vacancy-atom exchange mechanism

The profiles of the radial scans of the scaled structure factor can be seen in Fig. 9. The overlap of the different curves corroborates the scaling hypothesis. It is worth noting that scaling holds even at $q=0$, contrary to the case of atom-atom exchange mechanism at low quenching temperature. Scaling of data corresponding to different system sizes has also been checked. The continuous lines show fits of Lorentzian functions [Eq. (3.7)] with $\alpha=3/2$ and $\sigma=1$. The log-log plots shown in the insets of Fig. 9 reveal that, for large $\tilde{q}$, $\tilde{S}_r(\tilde{q})$ decays as $\tilde{q}^{-3}$, as indicated by the continuous line.

Figure 10 shows a log-log plot of the time evolution of $\sigma_r(t)$, $\langle\Delta E(t)\rangle$, and the best fits of the power laws defined by Eq. (4.2). The resulting x and y exponents, are listed in Table III, and plotted as a function of $1/L$ in Fig. 11. Extrapolations to $L\to\infty$ render $x\simeq y\simeq 0.36$ for $T_q=1.0J/k_B$ and $x\simeq y\simeq 0.44$ for $T_q=1.5J/k_B$.

The profiles of the transverse scan of the scaled structure factor are plotted in Fig. 12. Notice that the scaling is again satisfied at $q=0$. Scaling also holds for data corresponding to different system sizes. The continuous lines show fits of Lorentzian functions [Eq. (3.7)] with $\alpha=1$ and $\sigma=1$. The behavior of the tail is $\tilde{S}_t(\tilde{q})\propto\tilde{q}^{-2}$, as we obtained for the atom-atom exchange case.

The time evolution of $\sigma_t(t)$ can be seen in Fig. 13 and the fitted exponents according to Eq. (4.3) are plotted in Fig. 11 and listed in Table III. The extrapolations to $L\to\infty$ render $z\simeq 0.34$ for $T_q=1.0J/k_B$ and $z\simeq 0.44$ for $T_q=1.5J/k_B$.

V. DISCUSSION

The analysis of the growth exponents for finite L reveals that, independently of the mechanism and the temperature, the exponents x and y corresponding to $\langle\Delta E(t)\rangle$ and $\sigma_r(t)$, respectively, coincide within errors bars. The numerical value obtained at low temperature ($T_q=0.55T_0$) is, for both mechanisms, lower than the Allen-Cahn growth-exponent 1/2. This may be mainly attributed to the presence of planar (exactly zero curvature) interfaces, which is known to globally slow down the dynamics.[9] At the highest tem-

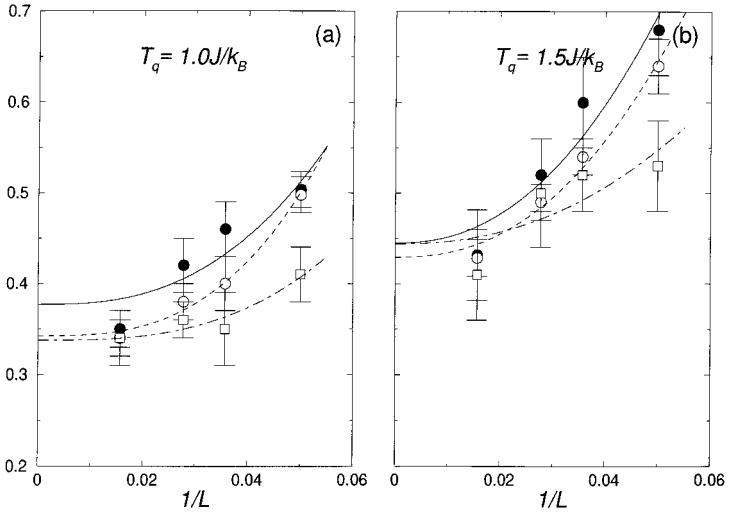

FIG. 11. Same as for Fig. 6 but for the vacancy-atom exchange mechanism.

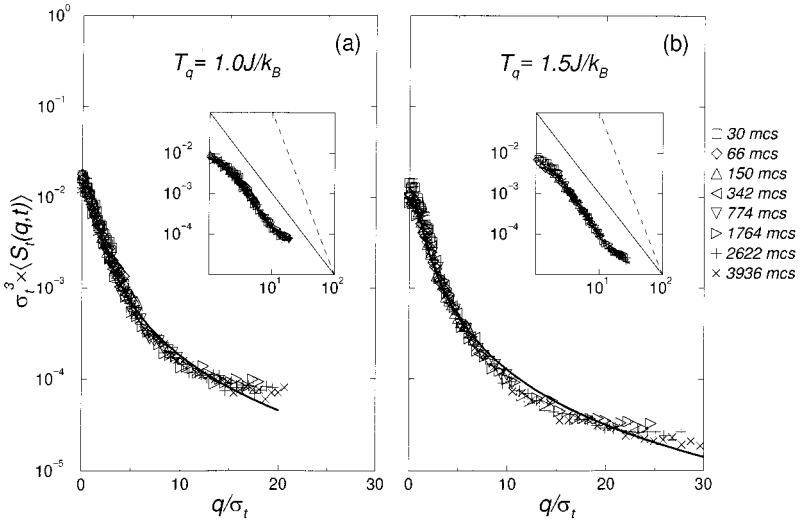

FIG. 12. Same as for Fig. 7 but for the vacancy-atom exchange mechanism.

perature considered in this study ($T_q = 0.83T_0$) we obtain that such numerical value for the exponents becomes larger and closer to the Allen-Cahn value. Indeed, one expects that as the temperature increases, the pinning effect of the planar interfaces becomes weaker enabling larger exponents.[41] Actually the value $y = 1/2$ has been obtained experimentally for Cu_3Au (Ref. 18) with high accuracy at quenching temperatures T_q ranging from $0.96T_0$ to $0.99T_0$ (our greatest simulated value is $T_q = 0.83T_0$).

Concerning the exponent z, characterizing the evolution of σ_t, we globally obtain the same behavior than for the other exponents. That is, z increases with temperature. However, the low temperature behavior, is such that $z < x \simeq y$ for the atom-atom exchange mechanism, whereas $z \simeq x \simeq y$ for the vacancy-atom exchange mechanism. When increasing temperature we obtain that, for both mechanisms, $z \simeq x \simeq y$. Experimentally, no clear differences have been observed between y and z.[18,42] This could be either due to the fact that the experiments are performed at temperatures too close to T_0 to observe any anisotropic effect, or that the relevant physical mechanism for the growth is closer to the vacancy-atom exchange. Notwithstanding, we suggest that experiments at low temperature would be interesting in order to definitively conclude about the potentially realistic vacancy mechanism.

From the values of the exponents obtained for different system sizes we have performed a finite-size analysis following the method proposed in Ref. 23. This analysis assumes a first-order correction to the asymptotic growth law according to

$$R(t) \sim t^n \left(1 - \frac{b}{t} \right), \tag{5.1}$$

where n stands for any of the growth exponents x, y, or z. This implies that the finite-size dependence of the exponent n_L follows:

$$n_L = n_\infty + bL^{-1/n_\infty}. \tag{5.2}$$

Fits of this equation to the obtained exponents are plotted (solid lines) in Figs. 6 and 11. The resulting values for n_∞ are shown in Tables II and III. These extrapolated values confirm the points discussed in the previous paragraph. The values of the first-order correction coefficient b are shown in Table IV. For the case of atom-atom exchange mechanism the sign of the coefficients b corresponding to the exponents

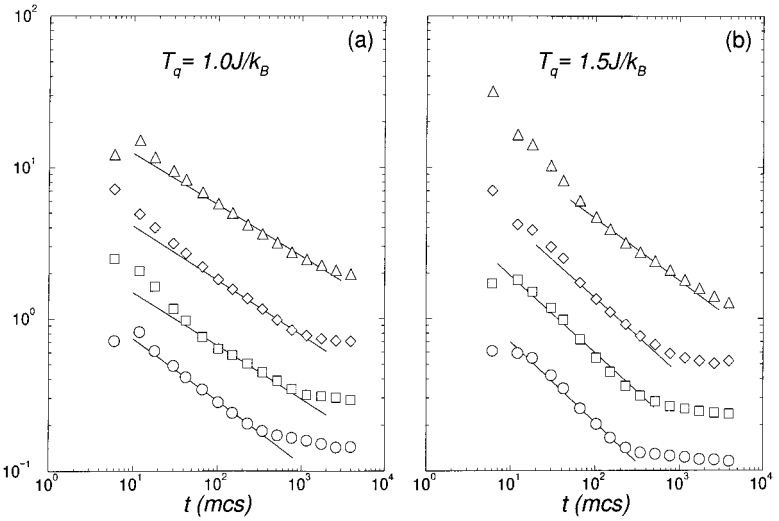

FIG. 13. Same as for Fig. 8 but for the vacancy-atom exchange mechanism.

TABLE III. Same as Table II for the vacancy-atom exchange mechanism.

k_BT_q/J	L	20	28	36	64	$L\to\infty$
1.0	ΔE	0.50±0.02	0.46±0.03	0.42±0.03	0.35±0.02	0.38±0.03
	σ_r	0.50±0.02	0.40±0.03	0.38±0.02	0.34±0.02	0.34±0.03
	σ_t	0.41±0.03	0.35±0.04	0.36±0.02	0.34±0.03	0.34±0.04
1.5	ΔE	0.68±0.05	0.60±0.05	0.52±0.04	0.43±0.05	0.44±0.05
	σ_r	0.64±0.03	0.54±0.02	0.49±0.02	0.43±0.02	0.43±0.03
	σ_t	0.53±0.05	0.52±0.04	0.50±0.06	0.41±0.05	0.44±0.06

z are negative reinforcing the suggestion that the growth law with the standard Allen-Cahn exponent does not hold in this case. It is also interesting to remark that, in general, the coefficient b is greater for the vacancy-atom exchange mechanism than for the atom-atom exchange one. This confirms that in the former case the exponents exhibit a greater dependence with finite size. This is in agreement with previous results reported for two-dimensional square lattices.[29]

Concerning the scaling of the structure factor, it is worth noting that it holds in a broad range of time for all the studied cases indicating that the domain-growth regime, in which the evolution of the system is governed by two characteristic lengths proportional, respectively, to σ_r^{-1} and σ_t^{-1}, is clearly reached in our simulations. Whether or not both lengths obey the same growth law can be detected by the scaling of the structure factor at $q=0$. At this q position, scaling holds only if $\sigma_r(t)\propto\sigma_t(t)$. For the case of vacancy-atom exchange mechanism, scaling at $q=0$ is satisfied, indicating that a single growth law governs the evolution of the system consistently with an unique value of the growth exponents ($x\simeq y\simeq z$). Contrary, for the case of atom-atom exchange mechanism, a lack of scaling at $q=0$ can be clearly seen in Figs. 4 and 7 (compare with Figs. 9 and 12 at $q=0$). This indicates that the two independent lengths are needed to characterize the evolution of the system in this case.

The time evolution of the structure factor at $q=0$ $[\langle S_r(q=0,t)\rangle=\langle S_t(q=0,t)\rangle=\langle(\Psi_1^2+\Psi_2^2+\Psi_3^2)/3\rangle]$, is shown in Fig. 14 for the two studied temperatures and for both mechanisms. They are in qualitative good agreement with the experimental results for Cu_3Au (see Fig. 18 in Ref. 18). Even the existence of a possible delay time due to an incubation period for nucleation, that has been found experimentally, can be observed as an inflection point in our curves. In our model the disordered phase is metastable down to zero temperature due to frustration effects.[32] Therefore the evolution, in our simulations, initiates via nucleation, as expected[37,38] for Cu_3Au in the experimentally studied temperature range.[18] Also in agreement with experiments, the delay time increases with increasing T_q. The experimentalists[18] suggest an explanation for this delay based on the influence of the elastic energy in the nucleation process. Although our model does not account for elastic effects it reproduces such results, indicating that a full explanation cannot rely only on elasticity arguments. Moreover, in Fig. 14, it seems that the delay is more important in the case of the vacancy mechanism. This problem will be studied in a future work.

The behavior of the tail of the structure factor along the radial and the transverse directions is markedly different. This can be clearly seen by comparing the insets of Figs. 4 and 9 corresponding to the radial scans and those of Figs. 7 and 12 corresponding to the transverse scans. For such anisotropic peaks, the Porod's Law,[39] $\langle S(q)\rangle\sim q^{-(d+1)}$, ($d+1=4$ in our case) is not expected to be satisfied. Independently of the dynamical exchange mechanism we have found that for large values of q, $\langle S_r(q)\rangle\sim q^{-3}$ and $\langle S_t(q)\rangle\sim q^{-2}$. This is in agreement with the fact that the best Lorentzian fits are obtained for $\alpha=3/2$ and $\alpha=1$ for radial and transverse scans, respectively, as explained in Sec. III. We have also studied the dependence of $\langle S(q)\rangle$ for large q along the diagonal direction $[\vec{k}=(1,1,0)+1/L\,(q,q,0)]$. Figure 15 compares the decay along this direction with the transverse and radial ones. For the diagonal direction, results are consistent with a q^{-3} decay. This reveals the singular character of the behavior along the transverse direction. It is interesting to remark that the present simulation results are not in agreement with the theory for ordering dynamics in Cu_3Au proposed by Lai.[19] In that theory it is found that the Porod's Law is satisfied for both radial and transverse scans. This important difference between Lai's theory and the present simulation probably arises from the fact that in our model type-1 walls have exactly zero excess energy.

In relation to the anisotropic character of the growth, we have obtained that, at low temperature, in the case of the atom-atom exchange mechanism two different lengths are needed whereas for the vacancy-atom exchange mechanism a single length is enough to describe the ordering process in fcc-A_3B alloys. Actually, for the case of atom-atom ex-

TABLE IV. Fitted coefficients b of Eq. (5.2).

k_BT_q/J		Atom-atom mechanism	Vacancy-atom mechanism
1.0	ΔE	98.7	386.1
	σ_r	45.4	1003.9
	σ_t	−1271.5	495.6
1.5	ΔE	31.2	212.3
	σ_r	106.2	233.3
	σ_t	−34.7	88.4

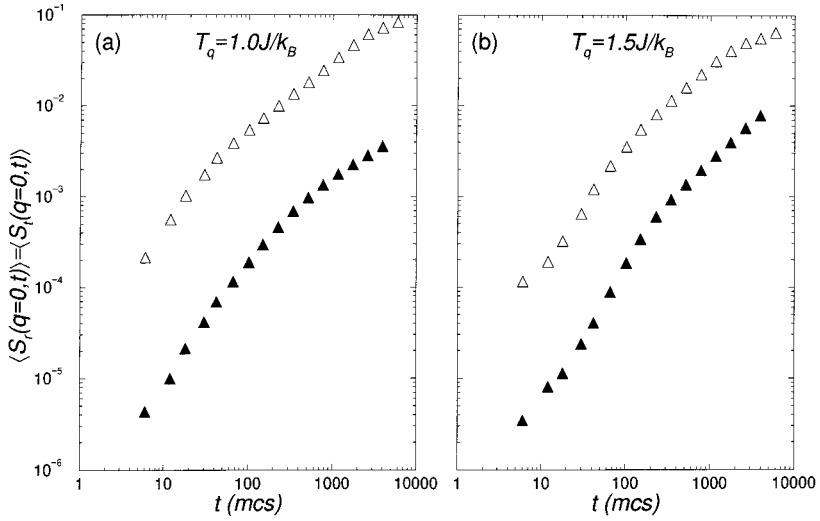

FIG. 14. Log-log plot of the value of the structure factor at the superstructure peak $q=0$ for a system with $L=64$ and two different quenching temperatures. Open symbols correspond to atom-atom exchange mechanism and filled symbols correspond to the vacancy-atom exchange mechanism.

change mechanism the need of two characteristic lengths is not surprising since it has been found in several studies on anisotropic growth. For instance, in a two-dimensional model for a martensitic transformation,[9] the existence of two relevant lengths arises as a consequence of the hierarchical evolution of a mixture of planar and curved interfaces present in the system. By hierarchical evolution one means that the curved interfaces have to wait for the planar ones to disappear before they can decrease in length. This kind of interrelated movement between walls is also present in our simulations. It is, however, worth mentioning that in the above mentioned model for martensitic transformation, the anisotropy is explicitly introduced in the Hamiltonian, while in the present case the anisotropy in the growth appears due to the topology of the fcc lattice. In Ref. 9 it is found, in quite good agreement with our results at low T_q using the atom-atom exchange mechanism, that the mean distance between planar interfaces grows as $t^{1/4}$ and that the mean distance between curved interfaces grows as $t^{1/2}$. Now, the question to be answered is: Why in the case of vacancy-atom exchange mechanism, the growth can be described by a single length? Before answering this question let us comment on some of the consequences of the vacancy-atom exchange mechanism on ordering dynamics. For two-dimensional square[40] and bcc lattices,[23] vacancies are known to accelerate the growth leading, at low temperatures, to an exponent greater than the Allen-Cahn 1/2. This is because when temperature decreases more vacancies are constrained to move preferentially along the interfaces so that the excitations become inhomogeneously distributed. As temperature increases, the excitations become homogeneous and the Allen-Cahn value is recovered. In the present model, the tendency for the vacancies to sit on the interfaces is quite low: some of the interfaces (type 1) are not energetic and, among the energetic ones (type 2), only those with an excess of the majority species represent a significant energy gain for the vacancies compared to the bulk. Then, as we obtain in our results, the acceleration of the domain growth process (compared to the atom-atom exchange mechanism) only shows up on the mean distance between type-1 walls due to a speed up in the motion of the curved walls (type 2). The reason why the evolution of type-2 walls is not sensitive to the dynamics is because it does not proceed independently: it is subordinated to the evolution of the type-1 walls. The consequence of this acceleration is that the interrelated wall movements can, in this case, be described by a single length.

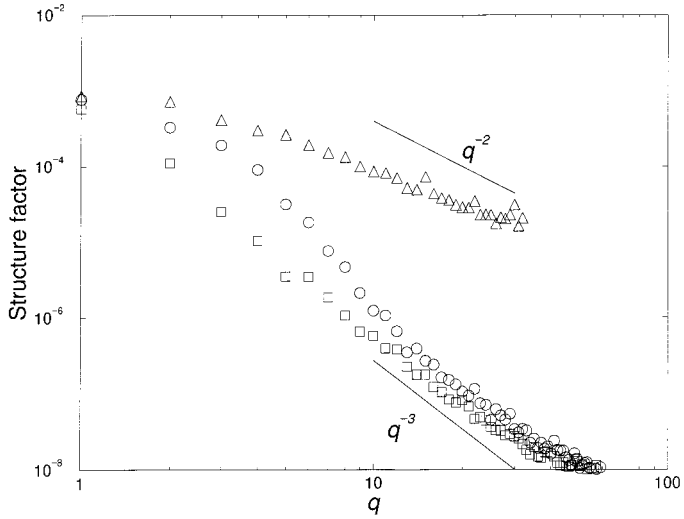

FIG. 15. Log-log plot of the structure factor decay in the radial (□), transversal (△), and diagonal (○) directions. Data, obtained with the atom-atom exchange mechanism, correspond to $t=1998$ mcs, $T_q=1.0J/k_B$, and $L=64$.

Concerning previous studies of the order-disorder dynamics by means of the vacancy-atom exchange mechanism we want to finally point out another important difference. In the case of the two-dimensional square lattice and bcc lattices the accelerations only appear if the vacancy has a finite probability to jump to NNN positions. Such jumps prevent the vacancy to be trapped in the ordered regions. When only jumps to NN positions are permitted, the growth becomes logarithmic (at low T_q). Although in the present simulations on fcc lattices we only allow vacancy jumps to NN positions, trapping does not appear since for such fcc lattices the ordered regions can be crossed without energy barriers. We have tested, by performing simulations allowing the vacancy to jump to NNN positions, that the growth exponents do not change significantly in this case.

VI. SUMMARY AND CONCLUSIONS

In this paper extensive Monte Carlo simulations of $L1_2$ ordering kinetics in a fcc A_3B binary alloy are presented. We have focused on the study of the evolution of the superstructure peak and the excess energy. We have followed the evolution up to 10^4 mcs in systems with linear sizes ranging from $L=20$ to $L=64$. Two different dynamics have been used: first the standard atom-atom exchange mechanism and second the more realistic vacancy-atom exchange mechanism. In this last case a very small concentration of vacancies is introduced in the system. Finite-size scaling techniques have been used in order to extrapolate to $L\rightarrow\infty$ the growth exponents evaluated at finite L. We have found that finite-size effects are more important in the case of the vacancy-atom exchange mechanism. For the atom-atom exchange mechanism we have found evidences for anisotropic growth at low T_q: the width of the superstructure peak in the transverse direction evolves according to $\sigma_t\sim t^{-z}$ with z smaller than the exponent y characterizing the evolution of the width in the radial direction $\sigma_r\sim t^{-y}$. Such anisotropy in the growth process has to do with the interrelated interface motion between the two different domain walls. As proposed in a recent theory,[9] this leads to $y=1/2$ and $z=1/4$ in rather good agreement with our present results. Contrary, for the vacancy-atom mechanism, the two relevant lengths σ_t^{-1} and σ_r^{-1} evolve following the same power-law. The disappearance of the anisotropic character in the growth when using the vacancy-atom exchange mechanism arises as a consequence of the speed up of type-2 (curved) interfaces which, in turn, accelerates the elimination of the type-1 (planar) interfaces. Moreover, the evolution of type-2 walls, always subordinated to the evolution of type-1 walls, does not seem to be sensitive to such acceleration. Finally, $\sigma_t\sim\sigma_r$ and a single length is enough to describe the ordering process.

The effect of the temperature has also preliminarily been studied. For both mechanisms the exponents y and z increase when the transition temperature is approached from below. To our knowledge, all the experiments have been performed at $T_q\sim T_0$, so that no conclusive results about the relevant ordering mechanisms can be deduced. The results in this paper suggest that more experimental studies of the ordering dynamics, especially at low temperatures, are desirable in order to clarify the existence of such anisotropic growth and which is the relevant mechanism for ordering. Synchrotron radiation facilities seem to be very promising for the obtainment of the needed structure factor maps in the late time regime.

ACKNOWLEDGMENTS

We acknowledge the Comisión interministerial de Ciencia y tecnología (CICyT) for financial support (Project No. MAT95-504) and the Fundació Catalana per a la Recerca (FCR) and the Centre de Supercomputació de Catalunya (CESCA) for computational facilities. C.F. also acknowledges financial support from the Comissionat per a Universitats i Recerca (Generalitat de Catalunya).

[1] J.D. Gunton, M. San Miguel, and P.S. Sahni, in *Phase Transitions and Critical Phenomena*, edited by C. Domb and J.L. Lebowitz (Academic, London, 1983).
[2] *Dynamics of Ordering Processes in Condensed Matter*, edited by S. Komura and H. Furukawa (Plenum, New York, 1988).
[3] G.F. Mazenko, Phys. Rev. B **43**, 8204 (1991).
[4] O.G. Mouritsen, Int. J. Mod. Phys. B **4**, 1925 (1990).
[5] D.A. Huse and C.L. Henley, Phys. Rev. Lett. **54**, 2708 (1985).
[6] E. Vives and A. Planes, Phys. Rev. Lett. **68**, 812 (1992).
[7] C. Frontera, E. Vives, T. Castán, and A. Planes, Phys. Rev. B **53**, 2886 (1996).
[8] S.M. Allen and J.W. Cahn, Acta Metall. **27**, 1085 (1979).
[9] T. Castán and P.-A. Lindgård, Phys. Rev. B **40**, 5069 (1989); **41**, 4659 (1990); **43**, 956 (1991).
[10] M.H. Marcinkowski and N. Brown, J. Appl. Phys. **32**, 375 (1961).
[11] G.E. Poquette and D.E. Mikola, Trans. Metall. Soc. AIME **245**, 743 (1969).
[12] M. Sakai and D.E. Mikola, Metall. Trans. A **2**, 1645 (1971).
[13] C.L. Rase and D.E. Mikola, Metall. Trans. A **6**, 2267 (1975).
[14] F. Bley and M. Fayard, Acta Metall. **27**, 1085 (1970).
[15] T. Hashimoto, K. Nishimura, and Y. Takeuchi, Phys. Lett. **65A**, 250 (1978).
[16] S. Katano, M. Iizumi, R.M. Nicklow, and H.R. Child, Phys. Rev. B **38**, 2659 (1988).
[17] S.E. Nagler, R.F. Shannon, C.R. Harkless, M.A. Singh, and R.M. Nicklow, Phys. Rev. Lett. **61**, 718 (1988).
[18] R.F. Shannon, Jr., S.E. Nagler, C.R. Harkless, and R.M. Nicklow, Phys. Rev. B **46**, 40 (1992).
[19] Z.-W. Lai, Phys. Rev. B **41**, 9239 (1990).
[20] J. Viñals and J.D. Gunton, Surf. Sci. **157**, 473 (1985).
[21] J.M. Cowley, J. Appl. Phys. **21**, 24 (1950).
[22] B. Fultz and L. Anthony, Philos. Mag. Lett. **59**, 237 (1989).
[23] C. Frontera, E. Vives, and A. Planes, Z. Phys. B **96**, 79 (1994).
[24] V. Yu, Dobretsov, G. Martin, F. Soisson, and V.G. Vaks, Europhys. Lett. **31**, 417 (1995).
[25] M. Porta and T. Castán, Phys. Rev. B **54**, 166 (1996).
[26] G. Van der Perre, H. Goeminne, R. Geerts, and J. Van der Planken, Acta Metall. **22**, 227 (1974); M. Guymont and D. Gratias, Acta Cryst. A **35**, 181 (1979); R.O. Williams, Metall. Trans. A **11**, 247 (1980).

[27] K. Yaldram and K. Binder, Z. Phys. B **82**, 405 (1991); J. Stat. Phys. **62**, 161 (1991); Acta Metall. Mater. **39**, 707 (1991).
[28] M. Blume, V.J. Emery, and R.B. Griffiths, Phys. Rev. A **4**, 1071 (1971).
[29] E. Vives and A. Planes, Int. J. Mod. Phys. C **4**, 701 (1993).
[30] W. Shockley, J. Chem. Phys. **6**, 130 (1938).
[31] R. Kikuchi, J. Chem. Phys. **60**, 1071 (1974).
[32] K. Binder, Phys. Rev. Lett. **45**, 811 (1980).
[33] B.E. Warren, *X-Ray Diffraction* (Dover, New York, 1990).
[34] R. Kikuchi and J.W. Cahn, Acta Metall. **27**, 1337 (1979).
[35] K. Binder, J. Comput. Phys. **59**, 1 (1985).
[36] See S. Amelinckx, in *Dislocations in Solids*, edited by F.R.N. Nabarro (North-Holland, Amsterdam, 1979), Vol. 2, p. 244.
[37] K.F. Ludwig, Jr., G.B. Stephenson, J.L. Jordan-Sweet, J. Mainville, Y.S Yang, and M. Sutton, Phys. Rev. Lett. **61**, 1859 (1988).
[38] B.D. Gaulin, E.D. Hallman, and E.C. Svensson, Phys. Rev. Lett. **64**, 289 (1990).
[39] G. Porod, in *Small Angle X-Ray Scattering*, edited by O. Glatter and L. Kratky (Academic, New York, 1982).
[40] C. Frontera, E. Vives, and A. Planes, Phys. Rev. B **48**, 9321 (1993).
[41] T. Castán and P.-A. Lindgård, Phys. Rev. B **41**, 2534 (1990).
[42] H. Berg and J.B. Cohen, Metall. Trans. **3**, 1797 (1971).